Article

Rigid MLGd (M = Fe, Ru) Complexes of a Terpyridine-Based Heteroditopic Chelate: A Class of Candidates for MRI Contrast Agents

Jrme Costa, Robert Ruloff, Lszl Burai, Lothar Helm, and Andr E. Merbach

J. Am. Chem. Soc., **2005**, 127 (14), 5147-5157• DOI: 10.1021/ja0424169 • Publication Date (Web): 19 March 2005

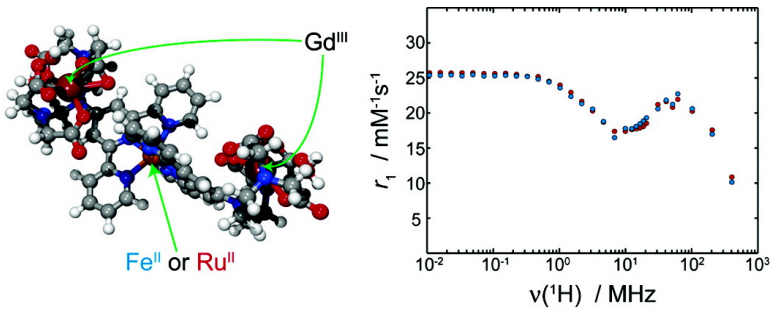

More About This Article

Additional resources and features associated with this article are available within the HTML version:

- Supporting Information
- Links to the 2 articles that cite this article, as of the time of this article download
- Access to high resolution figures
- Links to articles and content related to this article
- Copyright permission to reproduce figures and/or text from this article

View the Full Text HTML

J|A|C|S
ARTICLES
Published on Web 03/19/2005

Rigid $M^{II}L_2Gd_2^{III}$ (M = Fe, Ru) Complexes of a Terpyridine-Based Heteroditopic Chelate: A Class of Candidates for MRI Contrast Agents

Jérôme Costa, Robert Ruloff, László Burai, Lothar Helm, and André E. Merbach*

Contribution from the Ecole Polytechnique Fédérale de Lausanne (EPFL), Laboratoire de Chimie Inorganique et Bioinorganique, EPFL-BCH, CH-1015 Lausanne, Switzerland

Received December 17, 2004; E-mail: andre.merbach@epfl.ch

Abstract: Rigid chelates of high-molecular weight, $[M(tpy\text{-}DTTA)_2]^{6-}$ (M = Fe, Ru), are obtained upon self-assembly around one M^{II} ion of two terpyridine-based molecules substituted in the 4′-position with the polyaminocarboxylate diethylenetriamine-*N*,*N*,*N*′,*N*″-tetraacetate, tpy-$DTTA^{4-}$. The protonation constants of tpy-$DTTA^{4-}$ (log $K_1 = 8.65(4)$, log $K_2 = 7.63(4)$, log $K_3 = 5.25(6)$, log $K_4 = 3.30(7)$) and $[Fe(tpy\text{-}DTTA)_2]^{6-}$ (log $K_1 = 8.40(4)$, log $K_2 = 7.26(4)$) have been determined by potentiometry, ^{1}H NMR and UV−vis titrations. The thermodynamic stability constant log K_{GdL} of $[Fe(tpy\text{-}DTTA)_2Gd_2(H_2O)_4]$ measured at 25 °C by potentiometry is 10.87. This relatively low value is due to the direct linkage of the polyaminocarboxylate part to the electron-withdrawing terpyridine. UV−vis absorbance spectra of $[M(tpy\text{-}DTTA)_2Gd_2(H_2O)_4]$ and ^{1}H NMR spectra of $[M(tpy\text{-}DTTA)_2Eu_2(H_2O)_4]$ revealed similar solution behavior of the Fe and Ru complexes. An I_d water-exchange mechanism ($\Delta V^{\ddagger} = +6.8 \pm 1$ cm^3 mol^{-1}) with a rate constant of $k_{ex}^{298} = (5.1 \pm 0.3) \times 10^6$ s^{-1} has been found for $[Fe(tpy\text{-}DTTA)_2Gd_2(H_2O)_4]$ by ^{17}O NMR. A slow rotational correlation time ($\tau_{RO} = 410 \pm 10$ ps) and the presence of two water molecules ($q = 2$) in the coordination inner-sphere of each Gd^{III} ion have also been determined for this complex. A remarkably high relaxivity has been observed for both $[M(tpy\text{-}DTTA)_2Gd_2(H_2O)_4]$ complexes (at 20 MHz and 37 °C, $r_1 = 15.7$ mM^{-1} s^{-1} for the Fe complex, and $r_1 = 15.6$ mM^{-1} s^{-1} for the Ru complex).

Introduction

Gadolinium(III) DTPA- and DOTA-type chelates are successfully used as contrast agents for one of the most powerful techniques in medical diagnosis: magnetic resonance imaging (MRI). Microscopically, these contrast agents accelerate the NMR relaxation of surrounding water protons in soft tissue, which is enhancing the intrinsic contrast and thus the anatomical resolution of the magnetic resonance images. A measure for the efficacy of gadolinium(III) complexes for this process is the relaxivity value, defined as the longitudinal proton relaxation enhancement referred to 1 mM Gd^{3+} concentration. MRI contrast agents currently on the market have relaxivities around 4−5 mM^{-1} s^{-1}. Complexes with much higher relaxivities are a general item of interest for MRI investigations to monitor biological processes at the cellular and molecular level. In fact, relaxivities of more than 100 mM^{-1} s^{-1} can be attained according to the Solomon−Bloembergen theory when three of the most important influencing factors are simultaneously optimized: exchange rate of inner-sphere water molecules, rotation of the Gd−H vector (between gadolinium and protons of coordinated water), and electron spin relaxation of the paramagnetic center.[1] While it is difficult to influence the electron spin relaxation on a rational basis, a successful approach to tune the water exchange rate to its optimal value ($k_{ex} \approx 10^8$ s^{-1}) has been found by introducing a steric compression around the water binding site.[2,3] Optimizing the rotation of the Gd−H vector means to slow it down which is basically achieved by an increased molecular weight due to covalent or noncovalent binding of the gadolinium(III) chelate to a macromolecule. However, the improving effect of a higher molecular weight on relaxivity is significantly cut back by fast internal movements of the macromolecule itself or by local flexibility arising from the linker that binds the gadolinium(III) chelate to the macromolecular entity.

A promising approach to introduce more rigidity into the structure of contrast-enhancing complexes is the construction of self-assembling heterometallic systems with a well-defined rigid topology. We preliminary communicated the rational synthesis of the novel heteroditopic chelate tpy-$DTTA^{4-}$ that is based on a terpyridine unit substituted in the 4′-position with the polyaminocarboxylate diethylenetriamine-*N*,*N*,*N*″,*N*″-tetraacetate.[4] In aqueous solution in the presence of Fe^{II} and Gd^{III} ions, tpy-$DTTA^{4-}$ self-assembles in the trinuclear complex $[Fe(tpy\text{-}DTTA)_2Gd_2(H_2O)_4]$. A phenanthroline derivative of $[Gd(DO3A)(H_2O)_2]$ that self-assembles around one Fe^{II} to give a tetranuclear $Fe^{II}Gd_3^{III}$ structure has been described in a patent.[5]

(1) Tóth, É.; Helm, L.; Merbach, A. E. Relaxivity of Gadolinium(III) Complexes: Theory and Mechanism. In *The Chemistry of Contrast Agents in Medical Magnetic Resonance Imaging*; Tóth, É., Merbach, A. E., Eds.; Wiley: Chichester, 2001.
(2) Ruloff, R.; Tóth, É.; Scopelliti, R.; Tripier, R.; Handel, H.; Merbach, A. E. *Chem. Commun.* **2002**, 2630.
(3) Laus, S.; Ruloff, R.; Tóth, É.; Merbach, A. E. *Chem. Eur. J.* **2003**, *9*, 3555.
(4) Ruloff, R.; van Koten, G.; Merbach, A. E. *Chem. Commun.* **2004**, 842.

For both $Fe^{II}-Gd^{III}$ complexes, preliminary relaxivity data have been reported,[4,6] but no further details about the origin for an effective relaxation process have been evidenced thus far.

For this new class of candidates for MRI contrast agents, we report results of a study on structure and dynamics of the trinuclear complex $[Fe(tpy\text{-}DTTA)_2Gd_2(H_2O)_4]$ to gain deeper insights into favorable features of heterometallic self-assemblies to attain high relaxivities. Therefore, the three influencing factors, water exchange, rotation, and electron relaxation, were analyzed on the basis of multiple-field variable-temperature ^{17}O NMR and ^1H NMRD measurements. Moreover, we performed a thermodynamic study on ligand protonation and complex formation with regard to practical aspects of a safe application of $[Fe(tpy\text{-}DTTA)_2Gd_2(H_2O)_4]$ as MRI contrast agent.

We report furthermore the synthesis and results on structure and relaxivity of the Ru^{II} containing analogue of the $Fe^{II}Gd_3^{III}$ complex, namely $[Ru(tpy\text{-}DTTA)_2Gd_2(H_2O)_4]$, that is the first example of a Ru^{II}-based heterometallic assembly studied in the frame of investigations on MRI contrast agents.

Experimental Section

$[Ru(tpy\text{-}DTTA)_2]^{6-}$ Synthesis. Reagents used were purchased from commercial sources. The synthesis (Scheme 1) was performed under Ar and in D_2O to monitor the degree of complexation by ^1H NMR. All equipment was thoroughly oven dried and cooled under vacuum prior to reaction. tpy-$DTTA^{4-}$ and $[Ru(H_2O)_6](OTs)_2$ ($OTs^- = p$-toluenesulfonate anion) were synthesized according to the literature.[4,7]

In a round-bottomed flask, protected from light, 20 mL of D_2O were added to $[Ru(H_2O)_6](OTs)_2$ (0.22 mmol) with stirring. In a second flask, an excess of tpy-$DTTA^{4-}$ (0.61 mmol) was dissolved in 25 mL of D_2O. The pD was adjusted to 7.4 with 0.1 M NaOD. The Ru^{2+} solution was then slowly transferred to the ligand-containing solution that became rapidly dark red. After 1 h of continuous stirring at room temperature, the formation reaction was completed as indicated by ^1H NMR. NH_3 (4 mL of 1 M) was added, and the solution was filtered and evaporated to dryness. The remaining dark-red solid was dissolved in 20 mL of H_2O, and the pH was adjusted to 3.0 with 0.1 M HCl. This solution was loaded onto a cation-exchange column (Bio-Rad 50W-X4, H^+ form, 100 g). The column was washed with H_2O until neutral pH, and the product was eluted with 400 mL of 1 M NH_3. After evaporation and dissolution in 10 mL of 1 M NH_3, the red solution was loaded onto an anion-exchange column (Bio-Rad AG 1-X4, converted into $HCOO^-$ form, 90 g). The column was washed with H_2O until neutral pH. The product was eluted with HCOOH gradient (0.1−3 M), and $[Ru(tpy\text{-}DTTA)_2]^{6-}$ was collected with 1.5 M HCOOH as a red solution. The eluate was evaporated under reduced pressure to complete dryness and redissolved in H_2O. Evaporation and redissolution were repeated twice more to remove remaining formic acid. The red solid was dissolved in 3.6 g of D_2O, and the ruthenium content was quantified by ICP-AES, thus indicating a yield of 18.3 mg of $[Ru(tpy\text{-}DTTA)_2]^{6-}$ (0.015 mmol, 6.8% yield). ^1H NMR (400 MHz, D_2O, pD = 5.83): $\delta = 3.77$ (t, 8H), 3.97 (s, 16H), 4.39 (t, 8H), 7.17 (t, 4H [5,5″]), 7.54 (d, $J = 4.6$ Hz, 4H [6,6″]), 7.86 (t, 4H [4,4″]), 8.23 (s, 4H [3′,5′]), 8.53 (d, $J = 7.9$ Hz, 4H [3,3″]); MS (ESI) m/z: 615.2 (for $[RuH_4(tpy\text{-}DTTA)_2]^{2-}$).

A side product was collected in the 0.3 M HCOOH fraction of the anion-exchange chromatography consisting of decomposed $[Ru(tpy\text{-}DTTA)_2]^{6-}$. Analysis showed that one carboxylate arm was released from the complex, resulting in $[Ru(tpy\text{-}DTTA)(tpy\text{-}DT3A)]^{5-}$ (tpy-$DT3A^{3-}$ = 4′-(diethylenetriamino-*N*′,*N*′,*N*″-triacetate)-2,2′:6′,2″-terpyridine) whose isoelectric point is higher compared to that of $[Ru(tpy\text{-}DTTA)_2]^{6-}$. ^1H NMR (400 MHz, D_2O, pD = 4.28): $\delta = 3.60$ (t, 6H), 3.78 (t, 2H + s, 8H), 3.98 (s, 6H), 4.27 (t, 6H), 4.39 (t, 2H), 7.13 (m, 4H [5,5″]), 7.41 (m, 2H [6,6″]), 7.47 (m, 2H [6,6″]), 7.85 (m, 4H [4,4″]), 8.15 (s, 2H [3′,5′]), 8.18 (s, 2H [3′,5′]), 8.51 (m, 4H [3,3″]). Peak assignment results from relative integrals and 2D-COSY measurement (see Supporting Information); MS (ESI) m/z: 1176.3 for $[RuH_6(tpy\text{-}DTTA)(tpy\text{-}DT3A)]^+$.

Scheme 1. Synthesis of the $[M(tpy\text{-}DTTA)_2]^{6-}$ and $[M(tpy\text{-}DTTA)_2Ln_2(H_2O)_4]$ Complexes (M^{2+} = Fe^{2+}, Ru^{2+}; Ln^{3+} = Gd^{3+}, Eu^{3+})[a]

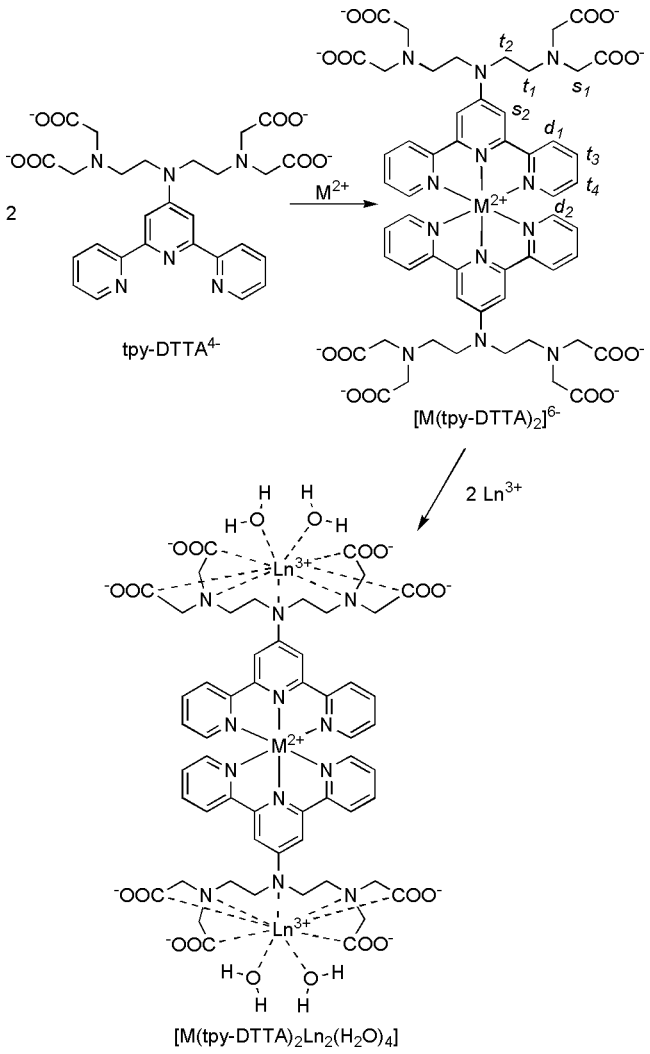

[a] For reaction conditions, refer to text.

Sample Preparation. The aqueous solutions of $[M(tpy\text{-}DTTA)_2Gd_2(H_2O)_4]$ (M^{II} = Fe^{II}, Ru^{II})[4] were prepared by mixing stoichiometric amounts of $Gd(ClO_4)_3$ and of the ligand $[M(tpy\text{-}DTTA)_2]^{6-}$. A slight excess of ligand was used, and the pH was adjusted to about 6 by adding NaOH. The solutions were allowed to react for 12 h at room temperature. All $[Fe(tpy\text{-}DTTA)_2Gd_2(H_2O)_4]$ solutions used in the ^{17}O NMR measurements had 2% $H_2{}^{17}O$ enrichment (IsoTrade GmbH, Mönchengladbach, Germany).

The tpy-$DTTA^{4-}$ and $[M(tpy\text{-}DTTA)_2]^{6-}$ solutions used in ^1H NMR were prepared by dissolving thoroughly dried solid samples in D_2O, and the pD was adjusted by use of NaOD and DCl solutions. The $[M(tpy\text{-}DTTA)_2Eu_2(D_2O)_4]$ used in ^1H NMR were prepared from solid ligands and $Eu_2(CO_3)_2$ dissolved in acidified D_2O. The pD was adjusted as above.

Potentiometry. The protonation constants of tpy-$DTTA^{4-}$ ($C_L = 3$ mM) and $[Fe(tpy\text{-}DTTA)_2]^{6-}$ ($C_L = 3$ mM) and the Gd^{III} stability

(5) Desreux, J. F.; Jacques, V.; Humblet, V.; Hermann, M.; Comblin-Tholet, V.; Tweedle, M. F. U.S. Patent 6,056,939, 2000; filed: 1998.
(6) Comblin, V.; Gilsoul, D.; Hermann, M.; Humblet, V.; Jacques, V.; Mesbahi, M.; Sauvage, C.; Desreux, J. F. *Coord. Chem. Rev.* **1999**, *185−186*, 451.
(7) Bernhard, P.; Biner, M.; Ludi, A. *Polyhedron* **1990**, *9*, 1095.

constants of $[Fe(tpy\text{-}DTTA)_2Gd_2(H_2O)_4]$ ($C_L = 3$ mM, $C_{Gd} = 6$ mM) were determined at $I = 0.1$ M (KCl) by pH potentiometric titration with KOH ($C_{KOH} = 50$ mM). The titrations were carried out using 3-mL sample solutions in a thermostated (25 ± 0.2 °C) glass-jacketed vessel with a magnetic stirrer (in an atmosphere of N_2 to avoid the effects of CO_2), with a Metrohm Dosimat 665 automatic buret and a combined glass electrode (C14/02-SC, reference electrode part Ag/AgCl in 3 M KCl, Moeller Scientific Glass Instruments, Switzerland) connected to a Metrohm 692 pH/ion meter. The hydrogen ion concentration was calculated from the measured pH values, as suggested by Irving, by using a correction term, obtained as the difference between the measured and calculated pH values in a titration of HCl (0.1 M) with standardized KOH.[8]

NMR Measurements. ^{17}O NMR spectra of $[Fe(tpy\text{-}DTTA)_2Gd_2(H_2O)_4]$ were recorded at variable temperature on Bruker Avance-600 (14.1 T, 81.3 MHz), Bruker DPX-400 (9.4 T, 54.2 MHz) and Bruker Avance-200 (4.7 T, 27.1 MHz) spectrometers. Bruker B-VT 3000 temperature control units were used to maintain a constant temperature, which was measured by a substitution technique.[9] Transverse and longitudinal ^{17}O relaxation rates and chemical shifts were measured for temperatures between 276.2 and 371.2 K ($C_{Gd} = 7.73$ mmol kg^{-1}). The samples were sealed in glass spheres adapted for 10-mm NMR tubes to avoid susceptibility corrections of the chemical shift.[10] Variable-pressure ^{17}O NMR measurements were performed up to 200 MPa with a home-built probehead[11] ($C_{Gd} = 3.08$ mmol kg^{-1}) on a Bruker ARX-400 (9.4 T, 54.2 MHz) spectrometer. The temperature was set to 276.8 K by circulating a thermostated liquid through the probe and was measured using a built-in Pt resistor. The longitudinal and transverse relaxation times, T_1 and T_2, were obtained with the inversion−recovery[12] and the Carr−Purcell−Meiboom−Gill[13] spin−echo techniques, respectively. Acidified water ($HClO_4$, pH = 3.7) was used as an external reference. Variable-pD ^1H NMR spectra of tpy-$DTTA^{4-}$ and $[Fe(tpy\text{-}DTTA)_2]^{6-}$ were recorded at room temperature (~21 °C) on a Bruker Avance-200 (4.7 T, 200 MHz) spectrometer. Concentration of each sample was 1 mM, and ionic strength was $I = 0.1$ M (NaCl). The pD were measured with a 5-mm Metrohm electrode that fits into a 5-mm NMR tube. One-dimensional (1D) and 2D TOCSY ^1H NMR spectra of $[Fe(tpy\text{-}DTTA)_2Eu_2(D_2O)_4]$ ($C_{Eu} = 1.2$ mM) and of $[Ru(tpy\text{-}DTTA)_2Eu_2(D_2O)_4]$ ($C_{Eu} = 4.7$ mM) were recorded on a Bruker DPX-400 (9.4 T, 400 MHz) spectrometer at pD = 6.35. The 1D spectrum of $[Ru(tpy\text{-}DTTA)_2Eu_2(D_2O)_4]$ and the 2D spectra of both complexes were recorded at 271.7 K and the 1D spectra of $[Fe(tpy\text{-}DTTA)_2Eu_2(D_2O)_4]$ between 271.7 and 371.7 K. The ^1H NMR spectra were all calibrated with H_2O (HDO) fixed at 4.80 ppm.

^1H NMRD Relaxivity. Longitudinal ^1H relaxation rates were measured at 278.2, 298.2, and 310.2 K on $[Fe(tpy\text{-}DTTA)_2Gd_2(H_2O)_4]$ ($C_{Gd} = 4.73$ mM, pH = 5.98) and at 298.2 and 310.2 K on $[Ru(tpy\text{-}DTTA)_2Gd_2(H_2O)_4]$ ($C_{Gd} = 0.80$ mM, pH = 5.87). The measurements were performed on a Stelar Spinmaster FFC relaxometer (fast field cycling: $2 \times 10^{-4} - 0.47$ T, corresponding to a proton Larmor frequency range of 0.01−20 MHz) equipped with a VTC90 temperature control unit, on a Bruker Minispec Console connected to 0.71 T (30 MHz), 0.94 T (40 MHz), and 1.41 T (60 MHz) permanent magnets, on a Bruker Avance-200 console connected to 1.18 T (50 MHz), 2.35 T (100 MHz), and 4.7 T (200 MHz) cryomagnets, and on a Bruker DPX-400 (9.4 T, 400 MHz). The samples were placed in cylindrical tubes. The diamagnetic corrections to the ^1H longitudinal relaxation rates were 0.55 s^{-1} (278.2 K), 0.37 s^{-1} (298.2 K), and 0.33 s^{-1} (310.2 K).

Spectrophotometric Titrations. Twenty-five milliliter titrations of tpy-$DTTA^{4-}$ ($C_L = 3.12 \times 10^{-5}$ M) and $[Fe(tpy\text{-}DTTA)_2]^{6-}$ ($C_L = 5.14 \times 10^{-5}$ M) samples were performed in a thermostated glass-jacketed vessel at 25 ± 0.2 °C with a magnetic stirrer, under a constant Ar flow, at $I = 0.1$ M (KCl), and with KOH as titrant ($C_{KOH} = 50$ mM). A J&M TIDAS-MMS UV/500-1 diode-array spectrometer coupled to a Hellma immersion probe (10-mm path length) was used to record spectra between 235 and 450 nm for tpy-$DTTA^{4-}$ and 430−700 nm for $[Fe(tpy\text{-}DTTA)_2]^{6-}$.

EPR. EPR spectra of $[Fe(tpy\text{-}DTTA)_2Gd_2(H_2O)_4]$ ($C_{Gd} = 4.73$ mM, pH = 5.98) were recorded in continuous-wave mode at Q-band on a Bruker Elexys E 500 spectrometer (35 GHz), at W-band on a Bruker Elexys E 680 spectrometer (95 GHz),[14] and on a quasi-optical spectrometer developed at the National High Magnetic Field Laboratory (Tallahassee, Florida) at higher frequencies. The instrument is similar to that of Smith et al.,[15] using a 108.5 GHz Gunn diode as a microwave source, and frequency multipliers allowing for 217 and 325 GHz, respectively.

Molecular Modeling. To assess the Gd−Gd distance in $[Fe(tpy\text{-}DTTA)_2Gd_2(H_2O)_4]$, a molecular model was built using the CAChe program,[16] where Gd^{III} was replaced for convenience by Sr^{II}. The structure was partially optimized using molecular mechanics (MM2 force field) and semiempirical calculations (PM5 method).

Data Analysis. The simultaneous least-squares fit of ^{17}O NMR and ^1H NMRD data as well as the protonation constants obtained by ^1H NMR were performed by the Visualiseur/Optimiseur programs on a Matlab platform, version 6.5.[17,18] The thermodynamic equilibrium constants and potentiometric protonation constants were calculated by the program PSEQUAD[19] and the p*M* by MEDUSA[20] The errors for the fitted parameters correspond to one standard deviation. The protonation constants obtained by spectrophotometry were computed by use of the Specfit[21] program. Differences between the measured and the computed absorbances were less than 7×10^{-3} absorbance unit at any wavelength. EPR spectra were analyzed by fitting Lorentzian functions using the NMRICMA program[22] for Matlab.

Results

Synthesis. We recently reported the synthesis of tpy-$DTTA^{4-}$ and the preparation of its $Fe^{II}Gd_2^{III}$ complex (Scheme 1).[4] The synthesis of $[Ru(tpy\text{-}DTTA)_2]^{6-}$ is more tedious than that of the Fe^{II} analogue due to fast ruthenium(II) oxidation in the presence of O_2. Rather than forming the Ru^{III} complex directly, followed by in situ reduction by a reducing agent, as is commonly the case for Ru^{II}−terpyridine complexes, we started from a hexaaqua ruthenium(II) salt,[7] avoiding numerous purification steps. After all solids, solvents, and glassware were thoroughly degassed, the complexation reaction took place at room temperature, under Ar atmosphere to avoid both oxidation from O_2 and N_2 fixation to Ru^{II}. The reaction was run at pH 7.0 and was complete after 1 h. Although low pH is usually preferred to slow the Ru^{II} oxidation rate,[23] we noticed that in

(8) Irving, H. M.; Miles, M. G.; Pettit, L. D. *Anal. Chim. Acta* **1967**, *38*, 475.
(9) Ammann, C.; Meier, P.; Merbach, A. E. *J. Magn. Reson.* **1982**, *46*, 319.
(10) Hugi, A. D.; Helm, L.; Merbach, A. E. *Helv. Chim. Acta* **1985**, *68*, 508.
(11) Cusanelli, A.; Nicula-Dadci, L.; Frey, U.; Merbach, A. E. *Inorg. Chem.* **1997**, *36*, 2211.
(12) Vold, R. L.; Waugh, J. S.; Klein, M. P.; Phelps, D. E. *J. Chem. Phys.* **1968**, *48*, 3831.
(13) Meiboom, S.; Gill, D. *Rev. Sci. Instrum.* **1958**, *29*, 688.
(14) Schmalbein, D.; Maresch, G. G.; Kamlowski, A.; Hofer, P. *Appl. Magn. Reson.* **1999**, *16*, 185.
(15) Smith, G. M.; Lesurf, J. C. G.; Mitchell, R. H.; Riedi, P. C. *Rev. Sci. Instrum.* **1998**, *69*, 3924.
(16) Fujitsu. *CAChe WorkSystem Pro 6.1*; 2000−2003.
(17) Yerly, F. *VISUALISEUR 2.3.4*; Université de Lausanne: Lausanne, Switzerland, 1999.
(18) Yerly, F. *OPTIMISEUR 2.3.4*; Université de Lausanne: Lausanne, Switzerland, 1999.
(19) Zekany, L.; Nagypal, I. *Computational Methods for Determination of Formation Constants*; Plenum Press: New York, 1985.
(20) Puigdomenech, I. *MEDUSA 25*; Royal Institute of Technology: Stockholm, Sweden, 1998.
(21) Binstead, R. A.; Zuberbühler, A. D.; Jung, B. *SPECFIT 3.06*; 1993−2004.
(22) Helm, L.; Borel, A.; Yerly, F. *NMRICMA 3.0.4*; EPFL: Lausanne, Switzerland, 2004.
(23) Aebischer, N.; Sidorenkova, E.; Ravera, M.; Laurenczy, G.; Osella, D.; Weber, J.; Merbach, A. E. *Inorg. Chem.* **1997**, *36*, 6009.

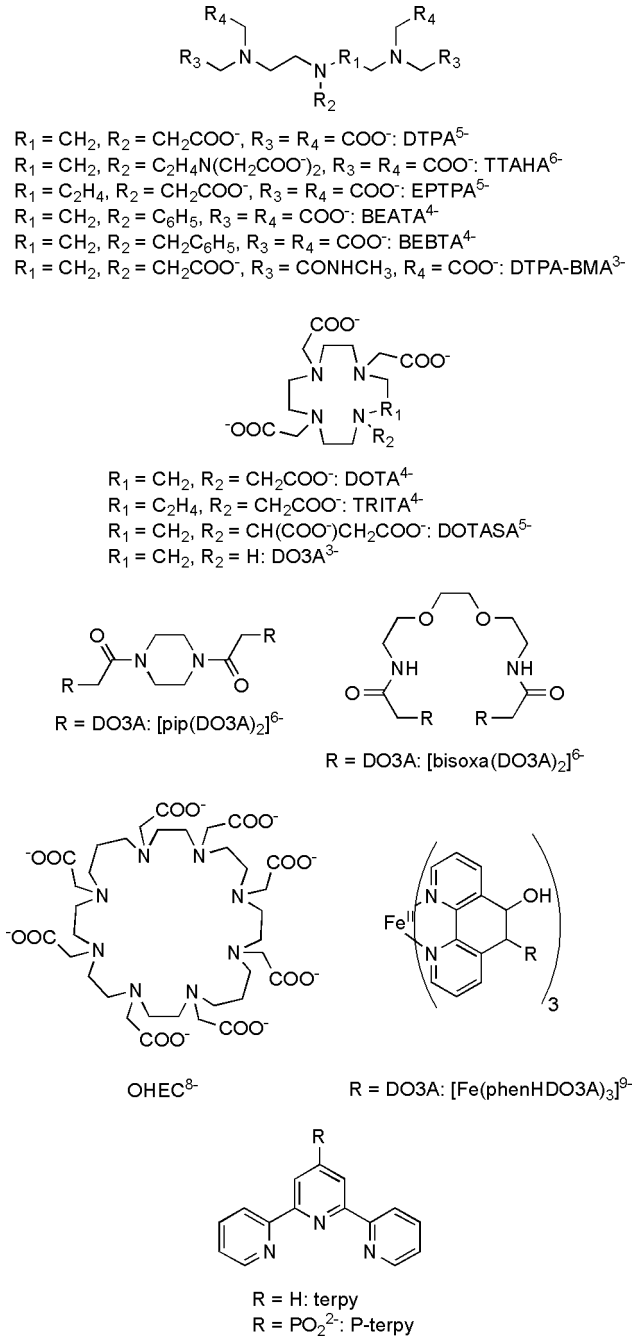

Figure 1. Structure of the ligands mentioned in the text.

acidic medium the complexation is also slower, thus increasing the probability of oxidation of the ruthenium(II) ion. Moreover, the log K_i values of tpy-DTTA^{4-} (see below) indicate that the terpyridine nitrogen atoms are deprotonated at neutral pH and, consequently, are readily available to complexation. Finally, a side product was obtained together with the desired [Ru(tpy-DTTA)$_2$]$^{6-}$, namely [Ru(tpy-DTTA)(tpy-DT3A)]$^{5-}$, in which one carboxylate arm was released from the complex. The relative yield of this side product was noticeably higher when working at low pH. Formation of the Ln^{III} complexes (Ln^{III} = Gd^{III}, Eu^{III}) took place as published for [Fe(tpy-DTTA)$_2$Gd$_2$(H$_2$O)$_4$] by mixing stoichiometric solutions of Ln(ClO$_4$)$_3$ and of the ligand.[4]

The tpy-DTTA^{4-} ligand is derived from tripod TTAHA (Figure 1) whose [C(NH$_2$)$_3$]$_3$[Gd(TTAHA)]·9H$_2$O X-ray crystal structure revealed a gadolinium ion coordinated by a N$_3$O$_4$ donor

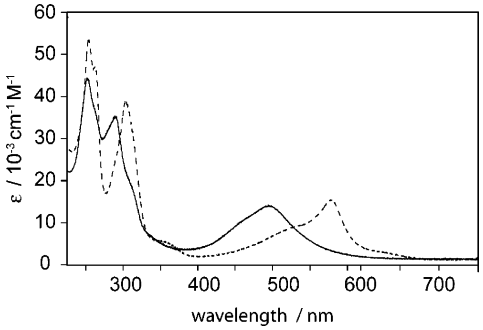

Figure 2. UV−vis absorbance spectra at room temperature in H$_2$O of [Ru(tpy-DTTA)$_2$Gd$_2$(H$_2$O)$_4$] (solid line) and [Fe(tpy-DTTA)$_2$Gd$_2$(H$_2$O)$_4$] (dashed line) at pH 5.95.

set and by two additional oxygen atoms from one carboxylate group of a neighboring similar complex.[24] In solution, two water molecules replace the oxygens of the neighboring complex.[25] In tpy-DTTA^{4-}, a terpyridine unit replaces the third pending arm of TTAHA.

The UV−vis absorbance spectra of both [M(tpy-DTTA)$_2$Gd$_2$(H$_2$O)$_4$] (M^{II} = Fe^{II}, Ru^{II}) in water are presented in Figure 2. Both spectra contain very intense bands in the UV region that can be assigned to ligand (tpy-DTTA)-centered $\pi \rightarrow \pi^*$ transitions. The relatively intense and broad absorption band in the visible region, which is responsible for the deep violet and red color of the Fe^{II} and Ru^{II} complexes, respectively, is due to the spin-allowed d $\rightarrow \pi$ metal-to-ligand charge transfer (MLCT) transition.[26] In a rigid matrix at 77 K, [Ru(terpy)$_2$]$^{2+}$ exhibits a strong, long-lived luminescence characteristic of a triplet metal-to-ligand charge transfer (^{3}MLCT) level. On increasing temperature, the luminescence intensity and lifetime decrease, and at room temperature, this compound is practically not luminescent.[26−31] Similarly, [Ru(tpy-DTTA)$_2$]$^{6-}$ and [Ru(tpy-DTTA)$_2$Gd$_2$(H$_2$O)$_4$] are not luminescent at room temperature in water.

Additional evidence of close resemblance of both [M(tpy-DTTA)$_2$Ln$_2$(H$_2$O)$_4$] (M^{II} = Fe^{II}, Ru^{II}) complexes is obtained through ^{1}H NMR. Each DTTA subunit is composed of four carboxylate and two ethylene functions, resulting in 16 protons that are in vicinity of the Ln^{III} ion. Figure 3 displays the spectra of both Eu^{III} complexes; as a result of the paramagnetic effects, the NMR signals of the protons close to europium(III) are substantially shifted from their diamagnetic positions. Eight peaks are counted between 8 and 28 ppm and eight more between −1 and −28 ppm at low temperature. The protons belonging to the terpyridine moiety are far from the Eu^{III} and therefore only slightly affected by the paramagnetic shift. Upon increase of the temperature, an exchange process takes place, leading to the coalescence of resonances. At high temperature,

(24) Ruloff, R.; Gelbrich, T.; Sieler, J.; Hoyer, E.; Beyer, L. *Z. Naturforsch., B: Chem. Sci.* **1997**, *52*, 805.
(25) Ruloff, R.; Muller, R. N.; Pubanz, D.; Merbach, A. E. *Inorg. Chim. Acta* **1998**, *275*−*276*, 15.
(26) Stone, M. L.; Crosby, G. A. *Chem. Phys. Lett.* **1981**, *79*, 169.
(27) Creutz, C.; Chou, M.; Netzel, T. L.; Okamura, M.; Suttin, N. *J. Am. Chem. Soc.* **1980**, *102*, 1309.
(28) Lin, C.-T.; Böttcher, W.; Chou, M.; Creutz, C.; Sutin, N. *J. Am. Chem. Soc.* **1976**, *98*, 6536.
(29) Young, R. C.; Nagle, J. K.; Meyer, T. J.; Whitten, D. G. *J. Am. Chem. Soc.* **1978**, *100*, 4773.
(30) Kirchhoff, J. R.; McMillin, D. R.; Marnot, P. A.; Sauvage, J.-P. *J. Am. Chem. Soc.* **1985**, *107*, 1138.
(31) Hacker, C. R.; Gushurst, A. K. I.; McMillin, D. R. *Inorg. Chem.* **1991**, *30*, 538.

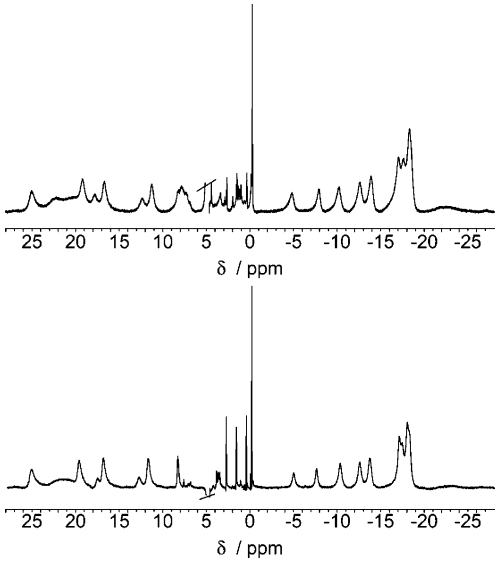

Figure 3. 400 MHz ^{1}H NMR spectrum at −1.5 °C of (top) [Ru(tpy-DTTA)$_2$Eu$_2$(H$_2$O)$_4$] and (bottom) [Fe(tpy-DTTA)$_2$Eu$_2$(H$_2$O)$_4$] at pH 5.95. The large water peak (cut) resonates at 4.8 ppm.

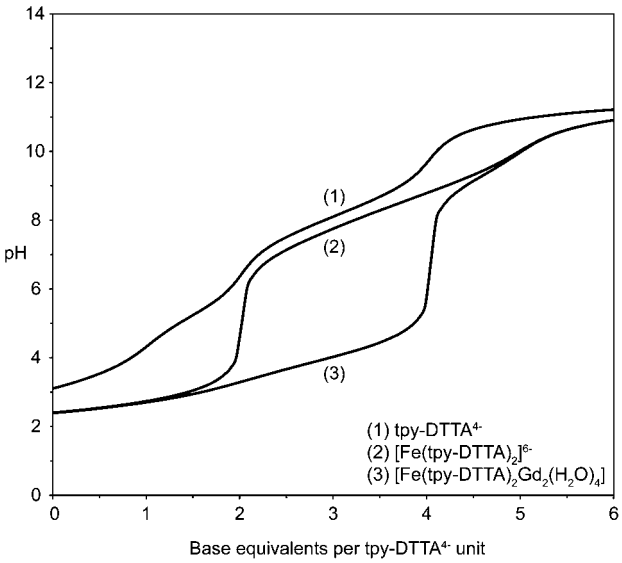

Figure 4. Titration curves at 25 °C and I = 0.1 M (KCl) of the tpy-DTTA^{4-} ligand, and the [Fe(tpy-DTTA)$_2$]$^{6-}$ and [Fe(tpy-DTTA)$_2$Gd$_2$(H$_2$O)$_4$] complexes.

only eight signals (four acetate, four ethylenic) of the same intensity are expected. A variable-temperature study of [Fe(tpy-DTTA)$_2$Eu$_2$(D$_2$O)$_4$] shows that at 98.5 °C the exchange process is still not in the fast-exchange limit. Figure 3 reveals that both [M(tpy-DTTA)$_2$Eu$_2$(D$_2$O)$_4$] complexes exhibit a similar ^{1}H NMR spectrum pattern with identical couplings, as proved by TOCSY cross-peaks. The structural and dynamic solution behavior of both Fe^{II} and Ru^{II} complexes are consequently very alike.

Protonation Constants. Protonation constants of tpy-DTTA^{4-} and [Fe(tpy-DTTA)$_2$]$^{6-}$ were first determined by potentiometry (Figure 4). The stepwise protonation constants K_n = [H$_n$L]/([H$_{n-1}$L][H$^+$]) were obtained by titration in the 2−12 pH range from the program PSEQUAD[19] and are summarized in Table 1. Note that the inflection point at basic pH on the titration curves of [Fe(tpy-DTTA)$_2$]$^{6-}$ and [Fe(tpy-DTTA)$_2$Gd$_2$(H$_2$O)$_4$] is due to the presence of ammonia, introduced through the use of Mohr's salt, (NH$_4$)$_2$Fe(SO$_4$)$_2$, as a source of Fe^{II}.

Table 1. Protonation and Stability Constants[a] for Various Ligands *L* and Their Gd^{III} Complexes

L		log K_1	log K_2	log K_3	log K_4	log K_{GdL}	log K_{GdHL}
tpy-DTTA^{4-}	*Pot*	8.65(4)	7.63(4)	5.25(6)	3.30(7)		
	NMR	8.87(4)	7.68(3)	5.15(1)	3.16(2)		
	UV	8.56(5)	7.44(5)	5.29(2)	3.04(4)		
[Fe(tpy-DTTA)$_2$]$^{6-}$	*Pot*	8.40(4)	7.26(4)			10.87(1)	3.73(3)
	NMR	8.30(5)	7.05(7)				
	UV	8.46(2)	7.07(2)				
TTAHA^{6-} [b]	*Pot*	10.66	8.56	8.38	2.92	19.0	8.3
DTPA^{5-}	*Pot*[c]	10.41	8.37	4.09	2.51	22.5	1.8
	NMR[d]	10.59	8.65	4.28	2.73		
P-terpy^{2-} [e]	*Pot*[f]	4.65	3.55				
	NMR[g]	4.64	3.30				
terpy	*Pot*[h]	4.64	3.42				

[a] *Pot* = data obtained through potentiometric titrations (25 °C, I = 0.1 M KCl), *NMR* = data obtained through ^{1}H NMR titrations (room temperature, I = 0.1 M NaCl), *UV* = data obtained through UV−visible titrations (25 °C, I = 0.1 M KCl). [b] There are also log K_5 = 2.39 and log K_6 = 2.0; ref 32. [c] There is also log K_5 = 2.04; ref 33. [d] 25 °C, I = 0.1 M KNO$_3$; there are also log K_5 = 2.06, log K_6 = 1.75, and log K_7 = 1.45; ref 34. [e] Only aromatic protons are displayed; ref 35. [f] 25 °C, I = 0.5 M KNO$_3$. [g] ^{1}H/^{31}P NMR, 25 °C, no control of I. [h] 25 °C, I = 0.1 M KNO$_3$; ref 36.

In comparison to DTPA^{5-} and TTAHA^{6-} (Figure 1), tpy-DTTA^{4-} has a much lower protonation constant for the first and second protonation steps. The loss of basicity of the nitrogen protonation sites in the aliphatic region with respect to DTPA^{5-} and TTAHA^{6-} is mainly due to the direct binding of this unit to the terpyridine moiety of the ligand. On tpy-DTTA^{4-} it is also possible to measure the first two protonation constants on the aromatic rings.

Several values ranging from 18.0 to 21.26 have been reported for the formation constant of [Fe(terpy)$_2$]$^{2+}$,[37−41] and we considered the Fe^{II} complex as totally formed in our pH working range. Due to the remoteness of the two tpy-DTTA^{4-} subunits in [Fe(tpy-DTTA)$_2$]$^{6-}$ we assumed that protonation occurs independently on both subunits. The system can therefore be regarded as twice R-(tpy-DTTA)$^{4-}$. Lowering of the two first log K_i's that was observed for tpy-DTTA^{4-} also applies in the case of the Fe(II)-complex, and as expected, only two nitrogen protonation constants could be found on the latter.

The ^{1}H NMR chemical shifts at different pH values were assigned on the basis of signal multiplicities, literature,[35,42] and 2D-COSY NMR spectrometry. Plots of the chemical shift values of the methylenic resonance of tpy-DTTA^{4-} and [Fe(tpy-DTTA)$_2$]$^{6-}$ as a function of pH are given in Figure 5. The pD values were obtained from the equation pD = pH + 0.4.[43] The proton NMR spectrum of the fully deprotonated tpy-DTTA^{4-}

(32) Ruloff, R.; Arnold, K.; Beyer, L.; Dietze, F.; Gründer, W.; Wagner, M.; Hoyer, E. *Z. Anorg. Allg. Chem.* **1995**, *621*, 807.
(33) *IUPAC Stability Constants 1.05*; Academic Software and K. J. Powell: Yorks, 1999.
(34) Letkeman, P.; Martell, A. E. *Inorg. Chem.* **1979**, *18*, 1284.
(35) Nazeeruddin, M. K.; Zakeeruddin, S. M.; Humphry-Baker, R.; Kaden, T. A.; Grätzel, M. *Inorg. Chem.* **2000**, *39*, 4542.
(36) Kim, K. Y.; Nancollas, G. H. *J. Phys. Chem.* **1977**, *10*, 948.
(37) Brandt, W. W.; Wright, J. P. *J. Am. Chem. Soc.* **1954**, *76*, 3082.
(38) Martin, R. B.; Lissfelt, J. A. *J. Am. Chem. Soc.* **1956**, *78*, 938.
(39) Holyer, R. H.; Hubbard, C. D.; Kettle, S. F. A.; Wilkins, R. G. *Inorg. Chem.* **1966**, *5*, 622.
(40) Bullock, J. I.; Simpson, P. W. G. *J. Chem. Soc., Perkin Trans. 1* **1981**, *77*, 1991.
(41) Schilt, A. A.; Wong, S.-W. *J. Coord. Chem.* **1984**, *13*, 331.
(42) Elsbernd, H.; Beattie, J. K. *J. Inorg. Nucl. Chem.* **1972**, *34*, 771.
(43) Mikkelsen, K.; Nielsen, S. O. *J. Phys. Chem.* **1960**, *64*, 632.

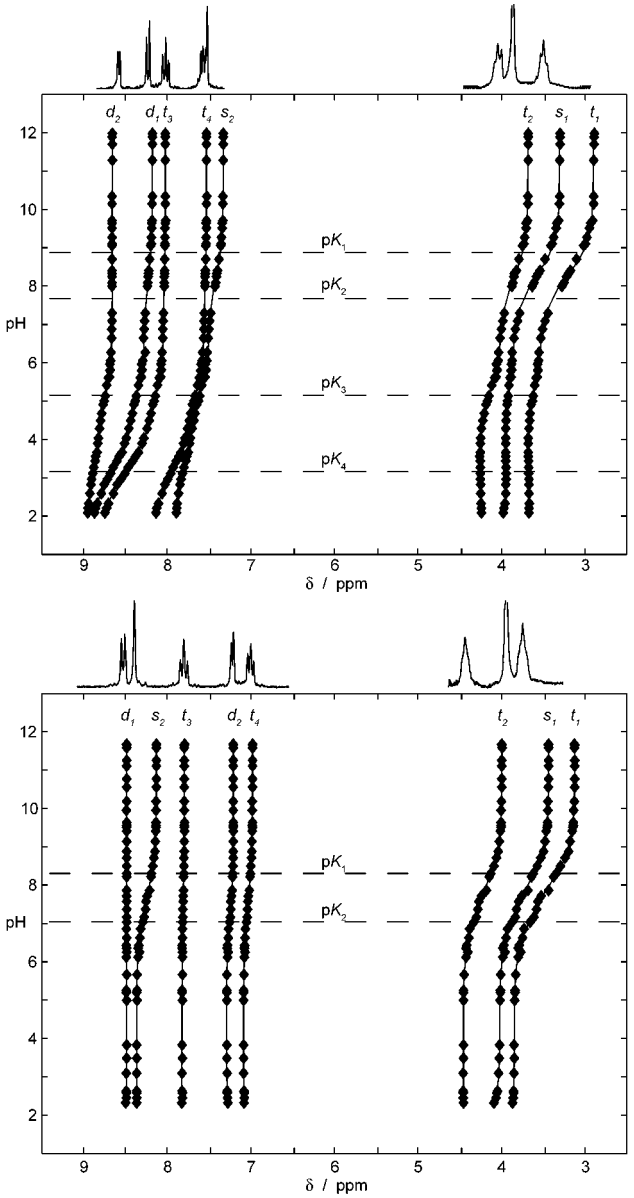

Figure 5. 200 MHz ^{1}H NMR titration at room temperature and $I = 0.1$ M (NaCl) of tpy-DTTA^{4-} (top) and [Fe(tpy-DTTA)$_2$]$^{6-}$ (bottom). The displayed spectra have been recorded at pH 6.27 (tpy-DTTA^{4-}) and 5.25 ([Fe(tpy-DTTA)$_2$]$^{6-}$). For signal labeling, see Scheme 1

ligand shows a lowest field doublet at $\delta = 8.66$ ppm, which is assigned to the d_2 proton (see Scheme 1 for numbering of the atoms), close to the chemical shift of the proton located at the same position in both P-terpy[35] and terpy.[42] The same similarity also applies for the triplets t_3 and t_4 at $\delta = 8.02$ and 7.53 ppm, respectively. Although some difference in the chemical shifts between the ligands arises from the d_1 doublet (8.18 ppm compared to 8.55 and 8.67 ppm for terpy and P-terpy), the most striking one occurs from the singlet proton on the central pyridine ring, s_2, on the β position to the central nitrogen of the polyaminocarboxylate group (8.47 on terpy, 8.3 on P-terpy, and 7.33 ppm on tpy-DTTA^{4-}). Upon coordination to Fe^{II} the d_2 proton of [Fe(tpy-DTTA)$_2$]$^{6-}$ is upfield shifted by more than one ppm ($\delta = 7.21$ ppm). This has already been observed for terpy[42] and bipy[44] and is explained by this proton being directed toward a high electronic density region composed of the t_{2g} electrons of the iron(II) and the π electrons of the pyridine rings and results in additional shielding of the nuclear spin. An inductive effect is postulated for the downfield shift of the d_1 proton ($\delta = 8.49$ ppm). On the aliphatic region, the singlet s_1 of the protons on the acetate arm and the triplets t_1 and t_2 of the ethylene are well separated. They all get deshielded on a similar way upon complexation of tpy-DTTA^{4-} to Fe^{II}: $\delta =$ 3.30−3.44 ppm for s_1, 2.89−3.13 for t_1, and 3.68− 4.00 for t_2.

The microscopic titration scheme obtained by ^{1}H NMR spectroscopy is indicative of the protonation sites. The protonation of a basic site leads to a deshielding of the adjacent proton (Figure 5).[45] Analysis of the pH dependence of the observed chemical shifts of the various protonated species δ_i^{obs} can be expressed as in eq 1:

$$\delta_i^{obs} = \sum_{n=1}^{N} \delta_{iH_nL} \times f_{H_nL} \qquad (1)$$

where δ_{iH_nL} is the intrinsic chemical shift of the i nucleus of the H_nL species and f_{H_nL} is the fractional population of each species. The protonation constants K_n are then related to the f_{H_nL} by eq 2:

$$K_n = \frac{f_{H_nL}}{f_{H_{n-1}L}[H^+]} \qquad (2)$$

On both tpy-DTTA^{4-} and [Fe(tpy-DTTA)$_2$]$^{6-}$ the aliphatic protons, s_1, t_1, and t_2, become deshielded at log K_1 and log K_2. The s_2 proton on the central aromatic ring at the β position from the central nitrogen of the DTTA subunit undergoes a similar deshielding, but the other pyridyl protons remain quite unaffected. This observation is coherent with a first protonation occurring on the central aliphatic nitrogen atom, and a second on one of the terminal aliphatic nitrogens, with displacement of the first proton from the central to the other terminal nitrogen atom, as was shown for DTPA^{5-} and EPTPA^{5-} (Figure 1).[34,46] Internal hydrogen bridges between the protonated terminal nitrogens and the deprotonated carboxylates stabilize the polyaminocarboxylate group of the molecule. Analogous to the aliphatic part, the protonation of the aromatic nitrogens of tpy-DTTA^{4-} occurs in the same manner: protonation of the central aromatic nitrogen (log K_3), followed by protonation on one of the lateral nitrogens with displacement of the central proton to the second lateral nitrogen (log K_4), as confirmed by the chemical shifts of the d_1, d_2, t_3, t_4, and s_2 protons. Protonation of the third aromatic nitrogen atom occurs below pH 2. Actually, down to pH 1.6, 2,2′-bipyridyl accepts only one proton[47] and P-terpy only two.[35] In comparison to P-terpy (Figure 1), log K_3 is slightly higher, even though both ligands have a group directly bound to the terpyridine unit. A strong electron-withdrawing behavior induces higher basicity on the nonadjacent rings of the terpyridine and results in a higher protonation constant.

The protonation constants of the tpy-DTTA^{4-} and [Fe(tpy-DTTA)$_2$]$^{6-}$ carboxylates could not be determined because they occur below pH 2. However, it can be seen in Figure 5 that the

(44) Castellano, S.; Gunther, H.; Ebersole, S. *J. Phys. Chem.* **1965**, *69*, 4166.
(45) Sherry, A. D.; Cacheris, W. P.; Kuan, K. T. *Magn. Reson. Med.* **1988**, *8*, 180.
(46) Wang, Y.-M.; Lee, C.-H.; Liu, G.-C.; Sheu, R.-S. *J. Chem. Soc., Dalton Trans.* **1998**, 4113.
(47) Baxendale, J. H.; George, P. *Trans. Faraday Soc.* **1950**, 55.

s_1 chemical shifts of both ligands start to move again downfield, as was the case during protonation of the aliphatic nitrogens.

The protonation constants were also determined by UV−visible spectrophotometry. The terpyridine moiety of the tpy-DTTA^{4-} ligand exhibits a strong absorption in the UV region below 400 nm with maximum absorbance at 287 nm (pH 2.40) shifting to 280 nm (pH 11.52). Protonation of the terpyridine nitrogen atoms induces drastic changes in the aromaticity as can be shown in Figure 6. In the 290−340 nm region, a shoulder is formed upon protonation of the aromatic protons, whereas protonation of the polyaminocarboxylate part has lower impact on the overall pattern of the spectra.

The [Fe(tpy-DTTA)$_2$]$^{6-}$ ligand is deeply violet in solution, and the visible spectrum exhibits a maximum at 569 nm (pH = 2.41) shifted to 574 nm (pH = 11.52) at slightly higher wavelength than the 552-nm maximum of [Fe(terpy)$_2$]$^{2+}$.[38,41] The results of the spectrophotometric titrations are also presented in Table 1.

Stability Constants. For the determination of the [Fe(tpy-DTTA)$_2$Gd$_2$(H$_2$O)$_4$] complex stability and protonation constants (K_{GdL} and K^{H}_{GdL}, respectively), the two DTTA subunits were also considered to be independent. K_{GdL} and K^{H}_{GdL} were determined by potentiometry and are defined in eq 3 as:

$$K_{GdL} = \frac{[GdL]}{[L][Gd^{3+}]}; \quad K^{H}_{GdL} = \frac{[GdHL]}{[GdL][H^{+}]} \qquad (3)$$

The titration curve is depicted in Figure 4, and the values of log K_{GdL} and log K^{H}_{GdL} are presented in Table 1. An indication of physiologically relevant complex stability is given by the pM values originating from the log K_{ML}. The pM values reflect the influence of the ligand basicity and the protonation of the complex at pH 7.4 and $[Gd]_{total} = 1\ \mu M$ and $[L]_{total} = 10\ \mu M$. The higher the pM, the more stable is the complex under these conditions. Table 2 indicates that the pGd of [Fe(tpy-DTTA)$_2$Gd$_2$(H$_2$O)$_4$] is lower than that of commercial contrast agents and of [Gd(TTAHA)(H$_2$O)$_2$]$^{3-}$.

To account for the low log K_{GdL} value several reasons can be invoked. The first one is that [Fe(tpy-DTTA)$_2$Gd$_2$(H$_2$O)$_4$] has one arm less than strong chelating linear polyaminocarboxylate complexes presented in Table 2, resulting in a less efficient wrapping procedure of the carboxylate arms around the Gd^{3+} ion. The direct binding of the aromatic part to the polyaminocarboxylate moiety also contributes to the low log K_{GdL}. The iron(II)-complexed terpyridine unit acts as a strong electron-withdrawing group, and the basicity of the lone-pair electron of the polyaminocarboxylate central nitrogen atom is reduced. This has already been observed by Tse and Powell when comparing the Gd^{III} formation constants of [Gd(BEATA)(H$_2$O)$_2$]$^-$ (pGd = 11.8)[51] and [Gd(BEBTA)(H$_2$O)$_2$]$^-$ (pGd = 16.1)[49] (see Figure 1 for the ligand structures).

^{17}O NMR and ^{1}H NMRD. The water exchange rate was determined for the Gd^{III} complex of the [Fe(tpy-DTTA)$_2$]$^{6-}$ ligand from a variable-temperature ^{17}O NMR study at three magnetic fields. Additionally, variable-temperature proton relaxation rates were measured on [Fe(tpy-DTTA)$_2$Gd$_2$(H$_2$O)$_4$] at three temperatures with the objective of determining parameters describing water exchange, rotation, electronic relaxation, and proton relaxivity. The experimental ^{17}O NMR and ^{1}H NMRD data were analyzed simultaneously (for equations, refer to the Appendix in the Supporting Information) and are shown together with the fitted curves in Figure 7.

At low temperatures, the ^{17}O reduced transverse relaxation rates increase with temperature. The exchange rate $k_{ex} = 1/\tau_m$ is directly determining $1/T_{2r}$ in this slow-exchange region. In the fast-exchange region (above 310 K), $1/T_{2r}$ is decreasing with temperature and is mainly determined by the transverse relaxation rate of the bound water oxygen, $1/T_{2m}$, which is influenced

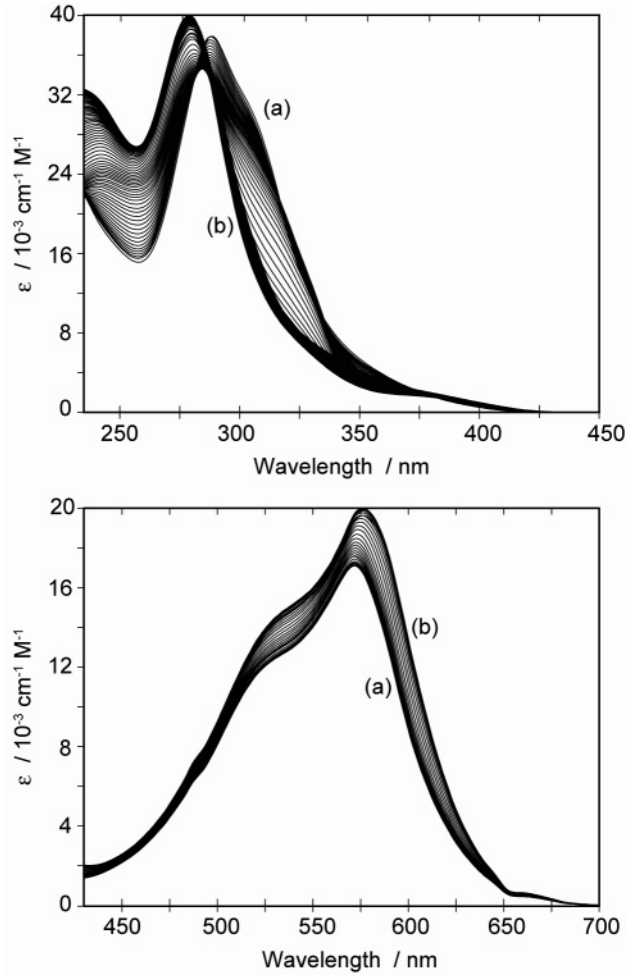

Figure 6. UV−visible absorbance spectra at 25 °C and $I = 0.1$ M (KCl) of (top) tpy-DTTA^{4-} from pH 2.43 (a) to pH 11.50 (b), and of (bottom) [Fe(tpy-DTTA)$_2$]$^{6-}$ from pH 2.41 (a) to pH 11.52 (b). For convenience, only 30 scans are displayed for the [Fe(tpy-DTTA)$_2$]$^{6-}$ titration.

Table 2. pM Values of GdL Complexes under Physiologically Relevant Conditions (pH 7.4; $[Gd]_{total} = 1\ \mu M$; $[L]_{total} = 10\ \mu M$); for Ligand Structures, See Figure 1

L	pGd	ref
DOTA^{4-} [a]	19.2	48
DTPA^{5-} [a]	19.1	33
BEBTA^{4-}	16.1	49
DTPA-BMA^{3-} [a]	15.8	50
TTAHA^{6-}	15.5	32
TRITA^{4-}	14.6	48
BEATA^{4-}	11.8	51
[Fe(tpy-DTTA)$_2$]$^{6-}$	10.6	this work

[a] Ligands of commercial contrast agents.

(48) Martell, A. E.; Motekaitis, R. J.; Clarke, E. T.; Delgado, R.; Sun, Y.; Ma, R. *Supramol. Chem.* **1996**, *6*, 353.
(49) Vasil'eva, V. F.; Lavrova, O. Y.; Dyatlova, N. M.; Yashunskii, V. G. *Zh. Obshch. Khim.* **1966**, *36*, 1724.
(50) Paul-Roth, C.; Raymond, K. N. *Inorg. Chem.* **1995**, *34*, 1408.
(51) Tse, P.-K.; Powell, J. E. *Inorg. Chem.* **1985**, *24*, 2727.

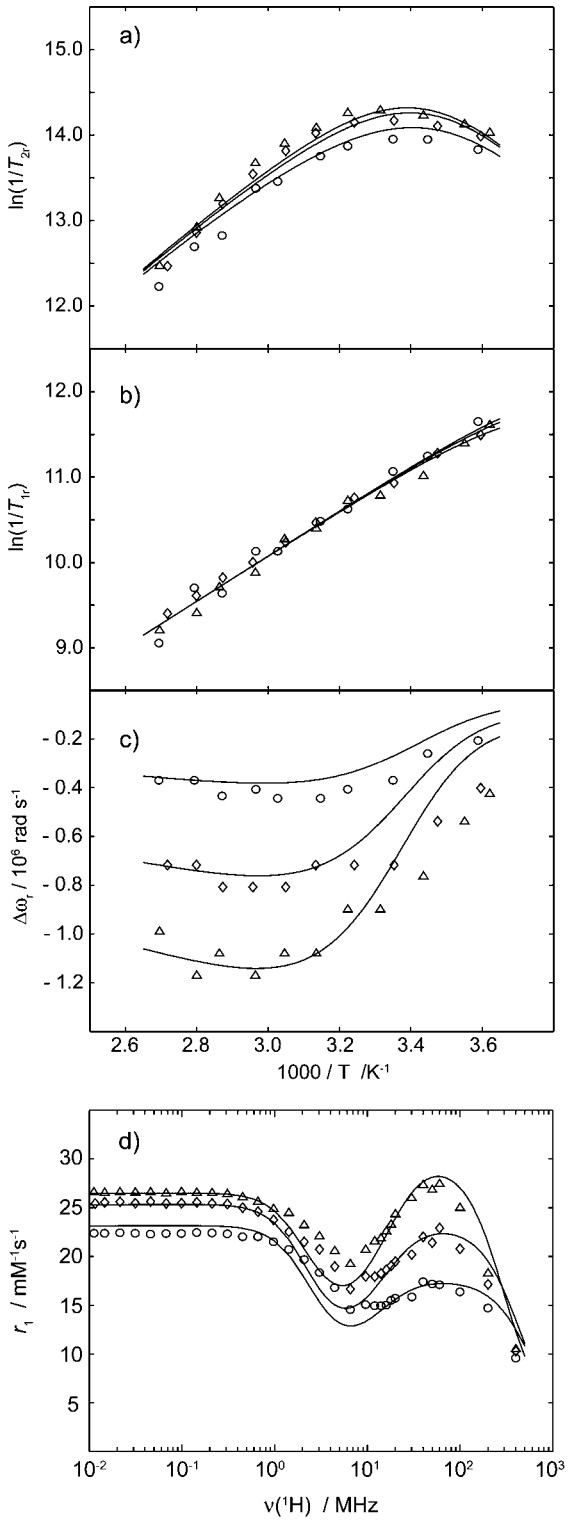

Figure 7. [Fe(tpy-DTTA)$_2$Gd$_2$(H$_2$O)$_4$] temperature dependence of reduced (a) transverse $1/T_{2r}$ and (b) longitudinal $1/T_{1r}$ ^{17}O relaxation rates; (c) ^{17}O chemical shifts $\Delta\omega_r$ at $B = 4.7$ T (○), 9.4 T (◇), 14.1 T (△); (d) ^{1}H NMRD profiles at 5 °C (△), 25 °C (◇), and 37 °C (○). The lines represent curves fitted to the experimental points.

by k_{ex}, the longitudinal electronic relaxation rate $1/T_{1e}$, and the hyperfine or scalar coupling constant, $A/\hbar$. The reduced ^{17}O chemical shifts are governed by $A/\hbar$ and, to a small extent, by an outer-sphere contribution characterized by C_{OS}, fixed to the common value of 0.1.[52,53] The ^{17}O longitudinal relaxation rate of water bound to Gd^{III} complexes in solution is dominated by

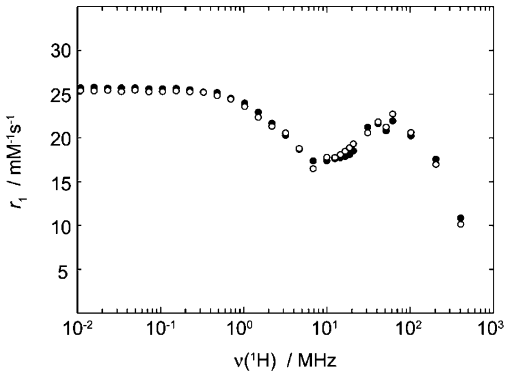

Figure 8. ^{1}H NMRD profiles at 25 °C of [Fe(tpy-DTTA)$_2$Gd$_2$(H$_2$O)$_4$] (○), and [Ru(tpy-DTTA)$_2$Gd$_2$(H$_2$O)$_4$] (●).

the dipole−dipole and quadrupolar relaxation mechanisms, and is only marginally influenced by k_{ex} at the lowest temperatures. $1/T_{1r}$ is characterized by the quadrupolar coupling constant, $\chi(1 + \eta^2/3)^{1/2}$, the rotational correlation time for the Gd^{III}−O vector, τ_{RO}, the activation energy for this rotational correlation, E_R, and the gadolinium(III)−oxygen distance, r_{GdO}.

The longitudinal ^{1}H relaxation rates were measured at three different temperatures and normalized to millimolar Gd^{III} concentration to obtain the longitudinal proton relaxivity, r_1, in mM^{-1} s^{-1}. The ^{1}H NMRD profiles are shown in Figure 7. At resonance frequencies below 1 MHz, we observed the characteristic plateau with r_1 being only slightly temperature dependent, while at frequencies between 10 and 200 MHz, a relaxivity hump caused by relatively slow rotational motion is found. Figure 8 presents the ^{1}H NMRD profiles at 25 °C of [M(tpy-DTTA)$_2$Gd$_2$(H$_2$O)$_4$] (M^{II} = Fe^{II}, Ru^{II}). It is interesting to remark that both compounds have an almost equal relaxivity over the whole range of frequencies. The only difference between the two complexes is chemical, with a higher kinetic inertness of the Ru^{II} center.

Electronic relaxation rates $1/T_{ie}$ ($i = 1, 2$) which influence both ^{17}O and ^{1}H NMR relaxation in Gd^{III} complexes are generally governed by the zero-field splitting (ZFS) term.[54−56] In the data analysis, we used Powell's approach[57] based on Solomon−Bloembergen−Morgan theory to calculate electron spin relaxation rates: $1/T_{ie}$ is given by transient ZFS, described by the trace of the squared ZFS tensor, Δ^2, and a correlation time, τ_v (with activation energy E_v), and a so-called spin rotation (SR) relaxation term, described by the deviations of the g Landé factor from the free electron value along the principal axes of the g_L tensor, δg_L^2.[53,57] A recent electronic relaxation theory developed by Rast and Borel involves both transient and static ZFS and describes electron spin relaxation with physically meaningful parameters.[58−60] Unfortunately, this analysis could

(52) Micskei, K.; Helm, L.; Brücher, E.; Merbach, A. E. *Inorg. Chem.* **1993**, *32*, 3844.
(53) González, G.; Powell, D. H.; Tissières, V.; Merbach, A. E. *J. Phys. Chem.* **1994**, *98*, 53.
(54) McLachlan, A. D. *Proc. R. Soc. London* **1964**, *A280*, 271.
(55) Powell, D. H.; Merbach, A. E.; González, G.; Brücher, E.; Micskei, K.; Ottaviani, M. F.; Köhler, K.; von Zelewsky, A.; Grinberg, O. Y.; Lebedev, Y. S. *Helv. Chim. Acta* **1993**, *76*, 1.
(56) Rast, S.; Fries, P. H.; Belorizky, E. *J. Chem. Phys.* **2000**, *113*, 8724.
(57) Powell, D. H.; Dhubhghaill, O. M. N.; Pubanz, D.; Helm, L.; Lebedev, Y. S.; Schlaepfer, W.; Merbach, A. E. *J. Am. Chem. Soc.* **1996**, *118*, 9333.
(58) Rast, S.; Borel, A.; Helm, L.; Belorizky, E.; Fries, P. H.; Merbach, A. E. *J. Am. Chem. Soc.* **2001**, *123*, 2637.
(59) Rast, S.; Fries, P. H.; Belorizky, E.; Borel, A.; Helm, L.; Merbach, A. E. *J. Chem. Phys.* **2001**, *115*, 7554.
(60) Dunand, F. A.; Borel, A.; Helm, L. *Inorg. Chem. Commun.* **2002**, *5*, 811.

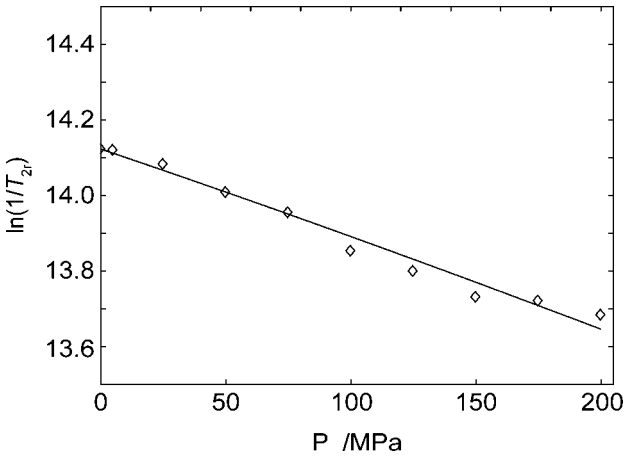

Figure 9. Pressure dependence of the reduced transverse 17O relaxation rates at $B = 9.4$ T for $[Fe(tpy\text{-}DTTA)_2Gd_2(H_2O)_4]$ at 3.6 °C. The line represents a curve fitted to the experimental points.

not be applied since we are lacking crucial EPR data for a wide range of magnetic fields and temperatures. In addition, $[M(tpy\text{-}DTTA)_2Gd_2(H_2O)_4]$ do not fit into the small-molecule constraints arising from the approximations involved in this model. A computer program to calculate ^{1}H NMRD profiles for slowly rotating complexes has been developed by Bertini et al.[61] The rotational correlation time of $[M(tpy\text{-}DTTA)_2Gd_2(H_2O)_4]$ is, however, too fast with respect to this model, and the experimental data could not be described in a satisfactory way.

The water-exchange mechanism can be assessed from variable-pressure ^{17}O transverse relaxation measurements by determining the activation volume, $\Delta V^{\ddagger}$, defined as the difference between the partial molar volume of the transition state and of the reactants.[62] The pressure dependence of $1/T_{2r}$ for $[Fe(tpy\text{-}DTTA)_2Gd_2(H_2O)_4]$ is shown in Figure 9. At 276.8 K, $1/T_{2r}$ is near the slow-exchange limit and therefore mainly dominated by k_{ex}. We included a possible pressure dependence of $1/T_{2m}$ ($\Delta V_m^{\ddagger} = \pm 5$ cm^3 mol^{-1}) in the fitting procedure and showed that it was negligible in the determination of the volume of activation for the water exchange, $\Delta V^{\ddagger}$. It is assumed that $A/\hbar$, δg_L^2, and the activation volume $\Delta V^{\ddagger}$ are independent of pressure.[52,53,63−65]

Discussion

All parameters obtained in the simultaneous fitting procedure are given in Table 3. From available crystal structures[24,66−68] and recent EPR results,[69] r_{GdO} has been fixed at 2.50 Å. The gadolinium(III)−proton distance, r_{GdH}, has been set to 3.10 Å[57,70] and the distance of closest approach of a second-sphere water proton to the Gd^{III} center, a_{GdH}, to 3.5 Å.[57] The obtained value of $-(3.7 \pm 0.1) \times 10^6$ rad s^{-1} for the scalar coupling constant, $A/\hbar$, is very similar to that obtained for other gadolinium complexes and confirms the initial assumption of two water molecules per gadolinium ion in the inner coordination sphere of the complex ($q = 2$), as found for $[Gd(TTAHA)(H_2O)_2]^{3-}$.[25] Since the measured ^{17}O longitudinal relaxation rates are in the fast-exchange region, they are mainly governed by $1/T_{1m}$ which itself depends on τ_{RO} through quadrupolar and dipolar relaxation mechanisms. The fitting procedure yielded a τ_{RO}^{298} value of 410 ± 10 ps for $[Fe(tpy\text{-}DTTA)_2Gd_2(H_2O)_4]$, which is ∼5 times higher than the value for the monomeric $[Gd(TTAHA)(H_2O)_2]^{3-}$. In general, internal motions lead to magnetic field dependence of ^{17}O $1/T_{1r}$ at low temperatures.[71] The absence of such a field dependence is indicative of the rigidity of $[Fe(tpy\text{-}DTTA)_2Gd_2(H_2O)_4]$: the only relevant internal motion corresponds to the rotation along the C−N axis of the polyaminocarboxylate subunit with respect to the Fe^{II}−terpyridine subunit. The value of 5.9 ± 1.6 MHz found for the quadrupolar coupling constant, $\chi(1 + \eta^2/3)^{1/2}$, is smaller than that of pure water (7.58 MHz).

The rate and the mechanism of water exchange are closely related to the inner-sphere solution structure of the complexes, and a $k_{ex}^{298} = (5.1 \pm 0.3) \times 10^6$ s^{-1} has been measured for the neutral $Fe(tpy\text{-}DTTA)_2Gd_2(H_2O)_4]$ (Table 3). The increase of the water-exchange rate of $[Gd(TTAHA)(H_2O)_2]^{3-}$ compared to that of $[Gd(DTPA)(H_2O)]^{2-}$ is due to the presence of the two water molecules in the inner-sphere of the complex, decreasing the stereorigidity of the system,[25] but is hardly affected by substituents that do not directly interfere in the inner coordination sphere.[52,53,72−74] The replacement of the third pending arm of the tripod TTAHA by the terpyridine unit of

Table 3. Parameters Obtained for $[Fe(tpy\text{-}DTTA)_2Gd_2(H_2O)_4]$ and Parent Gd^{III} Chelates from the Analysis of ^{17}O NMR and ^{1}H NMRD Data[a]

ligand	$[Fe(tpy\text{-}DTTA)_2]$	TTAHA[b]	DTPA[c]
$\Delta H^{\ddagger}$ [kJ mol^{-1}]	39.6 ± 1.4	40.4 ± 1.4	51.6 ± 1.4
$\Delta S^{\ddagger}$ [J mol^{-1} K^{-1}]	+16.4 ± 4.8	+23.3 ± 4.7	+53.0 ± 4.7
$\Delta V^{\ddagger}$ [cm^3 mol^{-1}]	+6.8 ± 1	+2.9 ± 1.0	+12.5 ± 0.2
k_{ex}^{298} [10^6 s^{-1}]	5.1 ± 0.3	8.6 ± 0.6	3.3 ± 0.2
τ_{RO}^{298} [ps]	410 ± 10	82 ± 5	58 ± 11
E_r [kJ mol^{-1}]	23 ± 1	19.9 ± 0.6	17.3 ± 0.8
$A/\hbar$ [10^6 rad s^{-1}]	−3.7 ± 0.1	−3.5 ± 0.1	−3.8 ± 0.2
$\chi(1 + \eta^2/3)^{1/2}$ [MHz]	5.9 ± 1.6	13 ± 1	14 ± 2
C_{OS}	*0.1*	*0.1*	0.18 ± 0.04
δg_L^2 [10^{-2}]	9.5 ± 0.2	2.0 ± 0.3	1.2 ± 0.3
τ_v^{298} [ps]	18.6 ± 0.4	25 ± 1	25 ± 1
E_v [kJ mol^{-1}]	*1*	*1*	1.6 ± 1.8
Δ^2 [10^{20} s^{-2}]	0.28 ± 0.01	0.34 ± 0.02	0.46 ± 0.02
D_{GdH}^{298} [10^{-10} m^2 s^{-1}]	*23*	16 ± 2	20 ± 3
E_{DGdH} [kJ mol^{-1}]	*25*	24.8 ± 1.5	19.4 ± 1.8
τ_{RH}/τ_{RO}	0.94 ± 0.04	*1*	*1*
q	*2*	*2*	*1*

[a] Values in italics were fixed in the fitting procedure. [b] Reference 25. [c] Reference 57.

(61) Bertini, I.; Galas, O.; Luchinat, C.; Parigi, G. *J. Magn. Reson.* **1995**, *113A*, 151.
(62) Lincoln, S. F.; Merbach, A. E. *Adv. Inorg. Chem.* **1995**, *42*, 1.
(63) Micskei, K.; Powell, D. H.; Helm, L.; Brücher, E.; Merbach, A. E. *Magn. Reson. Chem.* **1993**, *31*, 1011.
(64) Frey, U.; Merbach, A. E.; Powell, D. H. Solvent Exchange on Metal Ions: A Variable Pressure Approach. In *Dynamics of Solutions and Fluid Mixtures by NMR*; Delpuech, J.-J., Ed.; John Wiley & Sons: New York, 1995.
(65) Cossy, C.; Helm, L.; Merbach, A. E. *Inorg. Chem.* **1989**, *28*, 2699.
(66) Spirlet, M.-R.; Rebizant, J.; Desreux, J. F.; Loncin, M.-F. *Inorg. Chem.* **1984**, *23*, 359.
(67) Stezowski, J. J.; Hoard, J. L. *Isr. J. Chem.* **1984**, *24*, 323.
(68) Chang, C. A.; Francesconi, L. C.; Malley, M. F.; Kumar, K.; Gougoutas, J. Z.; Tweedle, M. F.; Lee, D. W.; Wilson, L. J. *Inorg. Chem.* **1993**, *32*, 3501.
(69) Raitsimring, A. M.; Astashkin, A. V.; Baute, D.; Goldfarb, D.; Caravan, P. *J. Phys. Chem. A* **2004**, *108*, 7318.
(70) Astashkin, A. V.; Raitsimring, A. M.; Caravan, P. *J. Phys. Chem. A* **2004**, *108*, 1990.
(71) Tóth, É.; Helm, L.; Kellar, K. E.; Merbach, A. E. *Chem. Eur. J.* **1999**, *5*, 1202.
(72) Tóth, É.; Burai, L.; Brücher, E.; Merbach, A. E. *J. Chem. Soc., Dalton Trans.* **1997**, 1587.
(73) Aime, S.; Geninatti Crich, S.; Gianolio, E.; Terreno, E.; Beltrami, A.; Uggieri, F. *Eur. J. Inorg. Chem.* **1998**, 1283.
(74) Tóth, É.; Connac, F.; Helm, L.; Adzamli, K.; Merbach, A. E. *Eur. J. Inorg. Chem.* **1998**, 2017.

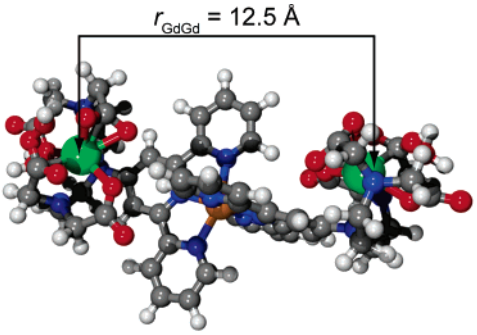

Figure 10. Ball-and-stick model of $[Fe(tpy\text{-}DTTA)_2Gd_2(H_2O)_4]$ by semiempirical calculations.

tpy-DTTA should not cause a significant change in the water exchange process. However, a high overall negative charge favors the leaving of a water molecule in a dissociative process, thus accelerating the exchange. Indeed, a 50% higher water-exchange rate was found for the pentacarboxylate DOTA derivative $[Gd(DOTASA)(H_2O)]^{2-}$ as compared to that for $[Gd(DOTA)(H_2O)]^{-}$.[75]

The exchange reaction is either slowed or accelerated by increasing pressure when $\Delta V^{\ddagger}$ is positive (dissociative activation mode) or negative (associative activation mode), respectively. A continuum of interchange I_d and I_a mechanisms exist between the *D* and *A* limiting mechanisms. The value of the activation volume found for $[Fe(tpy\text{-}DTTA)_2Gd_2(H_2O)_4]$, $\Delta V^{\ddagger} = +6.8 \pm 1$ cm^3 mol^{-1}, is intermediate between that of $[Gd(TTAHA)(H_2O)_2]^{3-}$ and $[Gd(DTPA)(H_2O)]^{2-}$ and indicates a dissociatively activated interchange I_d mechanism (Table 3). As for $[Gd(TTAHA)(H_2O)_2]^{3-}$, the difference with the commercial contrast agents lies in the number of inner-sphere water molecules, which is two instead of one.[25] The activation entropy $\Delta S^{\ddagger}$ and enthalpy $\Delta H^{\ddagger}$ of $[Fe(tpy\text{-}DTTA)_2Gd_2(H_2O)_4]$ also point to an I_d mechanism for the water exchange.

Putting two gadolinium(III) ions in close neighborhood may influence the electronic relaxation parameters of the complex: the intramolecular vicinity of two Gd^{III} ions can induce an increase of the transverse electronic relaxation rates, $1/T_{2e}$, and, consequently, a decrease in the relaxivity of the whole complex.[76] The crystallographic X-ray structure of $Na_2[Gd_2(OHEC)(H_2O)_2]\cdot 12H_2O$ (Figure 1) lead to a Gd−Gd distance of 6.5 Å,[77] and therefore a r_1 of only 3.5 mM^{-1} s^{-1} has been measured at 20 MHz and 37 °C for this complex.[76] We previously mentioned that the electronic relaxation rates mainly depend on ZFS. Following the approach of Powell et al.,[57] we introduced an additional intramolecular contribution to the electronic relaxation rates. This intramolecular part arises from the possible dipole−dipole interactions between the two gadolinium(III) ions of the complex. Attempts to obtain suitable crystals in order to determine r_{GdGd} have failed, and modeling has then been performed. Semiempirical calculations on $[Fe(tpy\text{-}DTTA)_2Sr_2(H_2O)_4]^{2-}$ revealed a Sr−Sr distance of 12.5 Å (Figure 10), which was assumed to be similar for Gd−Gd. At low magnetic fields, the electronic relaxation due to ZFS is dominant, while the intramolecular contribution gains importance at high fields

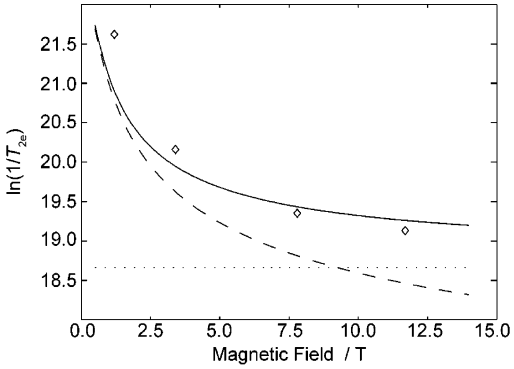

Figure 11. Comparison between experimental electronic relaxation times of $[Fe(tpy\text{-}DTTA)_2Gd_2(H_2O)_4]$ at room temperature (◇) and calculated values at 20 °C of zero-field splitting and spin rotation $1/T_{2e}$ (dashed line) and intramolecular $1/T_{2e}$ (dotted line) contributions, and their sum (solid line).

Table 4. Longitudinal Proton Relaxivities, r_1 in mM^{-1} s^{-1}, of Various Gd^{III} Polyaminocarboxylates, L, at 20 and 40 MHz (T = 37 °C); for Ligand Structures, See Figure 1

L	r_1^{20}	r_1^{40}	ref
$[Gd(DOTA)(H_2O)]^{-}$	3.8	3.5	57
$[Gd(DTPA)(H_2O)]^{2-}$	4.0	3.5	57
$[Gd(TTAHA)(H_2O)_2]^{3-}$	7.3	6.3	24/25
$[Gd_2(pip(DO3A)_2)(H_2O)_2]$	5.8	5.6	57
$[Gd_2(bisoxa(DO3A)_2)(H_2O)_2]$	4.9	4.4	57
$[Gd_2(OHEC)(H_2O)_2]^{2-}$	3.5	3.2	76
$[Fe(phenHDO3A)_3Gd_3(H_2O)_3]$	11.4	11.6	6
$[Fe(tpy\text{-}DTTA)_2Gd_2(H_2O)_4]$	15.7	17.4	this work
$[Ru(tpy\text{-}DTTA)_2Gd_2(H_2O)_4]$	15.6	17.3	this work

(Figure 11). A surprisingly good agreement was found between experimental values and the sum of all calculated contributions. We fitted again the ^{17}O NMR and ^1H NMRD data including this intramolecular contribution to the electronic relaxation rates. The parameters influencing the $1/T_{ie}$ did not vary significantly: τ_v^{298} raised to 22.3 ± 0.5 ps, while Δ^2 dropped to $(0.22 \times 10^{20}) \pm 0.01$ s^{-2}. The spin-rotation contribution slightly increased with $\delta g_L^2 = 0.1 \pm 0.02$. The diffusion energy E_{DGdH} was fitted and a value of 28.2 ± 1 kJ mol^{-1} was obtained.

The longitudinal ^1H relaxivity r_1 of iron(II) and ruthenium(II) $[M(tpy\text{-}DTTA)_2Gd_2(H_2O)_4]$ is high in the whole range of proton Larmor frequencies with respect to commercial MRI contrast agents. Table 4 compares the relaxivities of various complexes, and clearly shows that the bis(gadolinium)−M^{II} complexes are up to 10 times more efficient (5 times per Gd^{III}) in terms of relaxivity than clinically used $[Gd(DOTA)(H_2O)]^{-}$ and $[Gd(DTPA)(H_2O)]^{2-}$. It is noteworthy to mention that for today's high-field biological applications, this 10 times increase is still maintained at 200 MHz (at 37 °C, r_1 = 3.1 mM^{-1} s^{-1} for $[Gd(DTPA)(H_2O)]^{2-}$ and r_1 = 2.9 mM^{-1} s^{-1} for $[Gd(DOTA)(H_2O)]^{-}$). The benefit of two water molecules in the inner sphere of the Gd^{III} complex was already observed with the r_1 increase of $[Gd(TTAHA)(H_2O)_2]^{3-}$ compared to that of $[Gd(DTPA)(H_2O)]^{2-}$. Another feature of these complexes is the rigidity enhancement caused by the direct connection between the central aliphatic nitrogen and the 4′-carbon of the terpyridine to have the shortest and most rigid linker. Several other dinuclear complexes have been previously characterized, but their relaxivity enhancement due to a high molecular weight was counterbalanced by the flexibility of the whole system; $[Gd_2(pip(DO3A)_2)(H_2O)_2]$ and $[Gd_2(bisoxa(DO3A)_2)(H_2O)_2]$

(75) André, J. P.; Maecke, H. R.; Tóth, É.; Merbach, A. E. *J. Biol. Inorg. Chem.* **1999**, *4*, 341.
(76) Nicolle, G. M.; Yerly, F.; Imbert, D.; Böttger, U.; Bünzli, J.-C.; Merbach, A. E. *Chem. Eur. J.* **2003**, *9*, 5453.
(77) Schumann, H.; Boettger, U.; Weisshoff, H.; Ziemer, B.; Zschunke, A. *Eur. J. Inorg. Chem.* **1999**, 1735.

(Figure 1), among others,[78] have a loose connection between their two Gd^{III} ions, and the relaxivity gain with respect to that of the commercial Gd-DOTA monomer is therefore small (Table 4).[57] Another complex based on three phenanthroline-DO3A derivatives self-assembling around an Fe^{II} ion has been reported by Desreux and co-workers.[6] The resulting tris(gadolinium) complex exhibits high molecular weight and rigidity properties leading to an appreciable increase in relaxivity (Table 4), and was proposed as an Fe^{II}-responsive contrast agent. The found r_1 should, in principle, be even higher due to the size effect, but the gain is limited because of $q = 1$.

Recent studies on the rotation of Gd^{III} chelates showed that internal motions of the coordinated water molecules also have to be considered.[79,80] In the simultaneous treatment of ^{17}O NMR and ^1H NMRD results, the rotational correlation time of the $Gd-O_{water}$ vector, τ_{RO}, influencing longitudinal ^{17}O relaxation, and the rotational correlation time of the $Gd-H_{water}$ vector, τ_{RH}, influencing proton relaxivities, have been separated. Experimental studies[79] and molecular dynamics simulations[80] reached similar values for the ratio of these two rotational correlation times in different Gd^{III} complexes: $\tau_{RH}/\tau_{RO} = 0.65 \pm 0.2$. The ratio obtained in the present analysis is however close to 1 ($\tau_{RH}/\tau_{RO} = 0.94 \pm 0.04$), a value which results from the simultaneous analysis of ^{17}O NMR and ^1H NMRD data, without explicitly including a second coordination sphere. A possible explanation of $\tau_{RH}/\tau_{RO} \approx 1$ may arise from the constraints caused by the presence of two water molecules in the close vicinity of the Gd^{III} ion, inducing a restriction of the movements of the $Gd-H_{water}$ vector.

Conclusions

We report the physicochemical characterization of potential Gd^{III} MRI contrast agents, $[M(tpy\text{-}DTTA)_2Gd_2(H_2O)_4]$, (M = Fe, Ru), that self-assemble from M^{II} and two terpyridine derivatives functionalized with polyaminocarboxylate groups suitable for Ln^{III} complexation. The direct linkage of the polyaminocarboxylate moiety to the terpyridine part, although enhancing the rigidity of the Ln^{III} chelate, reduces the stability of the Gd^{III} complex.

The combined effect of two water molecules in the inner coordination sphere of the Gd^{III} complex, a slow rotational correlation time, and an extensive level of rigidity leads to high relaxivity at all ^1H NMRD frequencies for both Fe and Ru trinuclear complexes, when compared to the relaxivities of commercial medical MRI contrast agents and previously published dinuclear compounds. The water-exchange rate of $[Fe(tpy\text{-}DTTA)_2Gd_2(H_2O)_4]$ is characterized by an I_d mechanism and a small decrease in the rate constant compared to that of the parent $[Gd(TTAHA)(H_2O)_2]^{3-}$. Joining two gadolinium ions in the same compact complex leads to a higher density of paramagnetic species in a close environment which can also accelerate the electronic relaxation rates, thus lowering the relaxivity. However, semiempirical structural calculations and a remarkably high relaxivity confirm that this is not the case for $[Fe(tpy\text{-}DTTA)_2Gd_2(H_2O)_4]$.

The new Ru analogue, $[Ru(tpy\text{-}DTTA)_2Gd_2(H_2O)_4]$, possesses a solution behavior similar to that of the Fe complex. Although not luminescent at room temperature, it opens a way to a class of medical MRI contrast agents that are rigid and stable in solution, have a high molecular weight and a slow rotational correlation time, and could also act as luminescent probes. The synthesis and characterization of compounds belonging to this promising new era of multifunctional contrast agents are currently being investigated.

Acknowledgment. We are grateful to Meriem Benmelouka and Dr. Alain Borel for recording the EPR spectra. Dr. Alain Borel is also acknowledged for his help with the EPR spectra interpretation and molecular modeling. We are indebted to Fabrice Riblet for providing $[Ru(H_2O)_6](OTs)_2$. Finally, we thank Prof. Paul Dyson and Antoine Dorcier for their help with the ESI-MS. The Swiss National Science Foundation is acknowledged for financial support. This research was carried out in the frame of the European-funded EMIL program (LSHC - 2004 - 503569) and the EU COST Action D18.

Supporting Information Available: 1D variable-temperature ^1H NMR, 2D COSY ^1H NMR, and 2D TOCSY ^1H NMR spectra, variable-pH ^1H NMR spectra, proton relaxivities as a function of magnetic field and temperature, transverse and longitudinal ^{17}O relaxation rates and chemical shifts, EPR spectra, equations. This material is available free of charge via the Internet at http://pubs.acs.org.

JA0424169

(78) Ranganathan, R. S.; Fernandez, M. E.; Kang, S. I.; Nunn, A. D.; Ratsep, P. C.; Pillai, K. M. R.; Zhang, X.; Tweedle, M. F. *Invest. Radiol.* **1998**, *33*, 779.
(79) Dunand, F. A.; Borel, A.; Merbach, A. E. *J. Am. Chem. Soc.* **2002**, *124*, 710.
(80) Yerly, F.; Hardcastle, K. I.; Helm, L.; Aime, S.; Botta, M.; Merbach, A. E. *Chem. Eur. J.* **2002**, *8*, 1031.